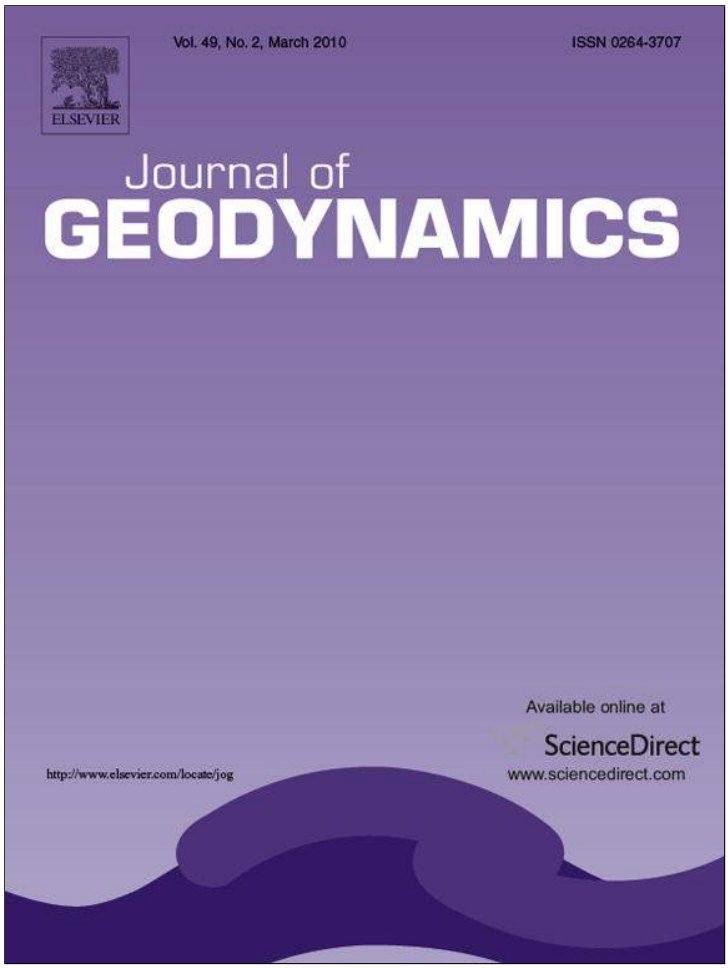

Journal of Geodynamics 49 (2010) 68–78

Contents lists available at ScienceDirect

Journal of Geodynamics

journal homepage: http://www.elsevier.com/locate/jog

Crustal velocity structure in the southern edge of the Central Alborz (Iran)

A. Abbassi [a], A. Nasrabadi [a], M. Tatar [a,*], F. Yaminifard [a], M.R. Abbassi [a], D. Hatzfeld [b], K. Priestley [c]

[a] International Institute of Earthquake Engineering and Seismology (IIEES), 26, Arghavan St., Dibajie Shomali, Farmanieh, 19537-14476 Tehran, Iran
[b] Laboratoire de Geophysique Interne et Tectonophysique, UJF-CNRS, 38400 Grenoble Cedex 9, France
[c] Bullard Laboratories, Cambridge CB3 OEZ, UK

ARTICLE INFO

Article history:
Received 1 February 2009
Received in revised form 9 September 2009
Accepted 23 September 2009

Keywords:
Central Alborz
1D inversion
Receiver function
Iran
Crustal structure
Rayleigh wave

ABSTRACT

Inversion of local earthquake travel times and joint inversion of receiver functions and Rayleigh wave group velocity measurements were used to derive a simple model for the velocity crustal structure beneath the southern edge of the Central Alborz (Iran), including the seismically active area around the megacity of Tehran. The P and S travel times from 115 well-located earthquakes recorded by a dense local seismic network, operated from June to November 2006, were inverted to determine a 1D velocity model of the upper crust. The limited range of earthquake depths (between 2 km and 26 km) prevents us determining any velocity interfaces deeper than 25 km. The velocity of the lower crust and the depth of the Moho were found by joint inversion of receiver functions and Rayleigh wave group velocity data. The resulting P-wave velocity model comprises an upper crust with 3 km and 4 km thick sedimentary layers with P wave velocities (V_p) of ~5.4 and ~5.8 km s^{-1}, respectively, above 9 km and 8 km thick layers of upper crystalline crust (V_p ~6.1 and ~6.25 km s^{-1} respectively). The lower crystalline crust is ~34 km thick (V_p ~ 6.40 km s^{-1}). The total crustal thickness beneath this part of the Central Alborz is 58 ± 2 km.

1. Introduction

The Central Alborz forms an active orogenic belt located on the southern margin of the South Caspian Basin North of Iran (Fig. 1). The kinematics, structure and evolution of the Central Alborz are of particularly interest because of the high seismic hazard they pose for the megacity of Tehran, with its population of more than 12 million. Because of the lack of large earthquakes (and detailed seismic analysis) during modern times, little is known about the structure and the kinematics of this active region.

The Central Alborz accommodates roughly 5 ± 2 mm/yr of shortening and 4 ± 2 mm/yr of left lateral strike–slip motion (Vernant et al., 2004). Seismicity (Jackson et al., 2002) and tectonic observations (Allen et al., 2003; Ritz et al., 2006) suggest that the overall oblique left-lateral motion across the Alborz is partitioned onto separate strike–slip and thrust faults, both parallel to the trend of the belt.

Very little is known about the crustal structure and the Moho depth of the Central Alborz. The first crustal thickness variations computed from surface wave analysis of a few events by Asudeh (1982) suggested a crustal thickness of 45 km beneath the Alborz mountain range, but that may not represent the crustal structure of the Central Alborz. Other crustal thickness estimations have been computed from Bouguer anomaly modeling by Dehghani and Makris (1984) for the whole of Iran. They showed that the Bouguer gravity along the Alborz mountain range varies between −100 and −120 mgal implying a crustal thickness of less than 35 km. Javan Doloei and Roberts (2003) estimated a crustal thickness of 46 ± 2 km beneath seven stations of Iranian Long Period Array (ILPA) located south-west of the Central Alborz using receiver function analysis.

Radjaee (2007), Radjaee et al. (submitted for publication) and Rham (2009) showed that the crust of the southern part of the Central Alborz has a thickness of about 52–54 km. They jointly inverted receiver functions and surface wave data using teleseismic events recorded by 26 temporary broadband stations operated for about 7 months in the Central Alborz. Paul et al. (submitted for publication) estimated the same thickness for the crust of the Central Alborz using receiver functions alone. All these studies indicate a small increase in crustal thickness (about 5 km) toward the southern flank of the Central Alborz, consistent with the Bouguer anomalies of Dehghani and Makris (1984). A more recent study by Sodoudi et al. (2009), based on receiver functions, indicates a crustal thickness of ~51–54 km beneath the Central Alborz and an unusual thickness of about 67 km beneath the Damvand volcano located on southern flank of the range.

In this paper, we used data from a temporary local network of 49 portable seismological stations operated from June to December 2006. This network was installed in the southern foothills of the Central Alborz, which is the most active region in the range and which contains the megacity of Tehran. We also used local

* Corresponding author.
E-mail addresses: mtatar@iiees.ac.ir, mtatar17@yahoo.com (M. Tatar).

0264-3707/$ – see front matter © 2009 Elsevier Ltd. All rights reserved.
doi:10.1016/j.jog.2009.09.044

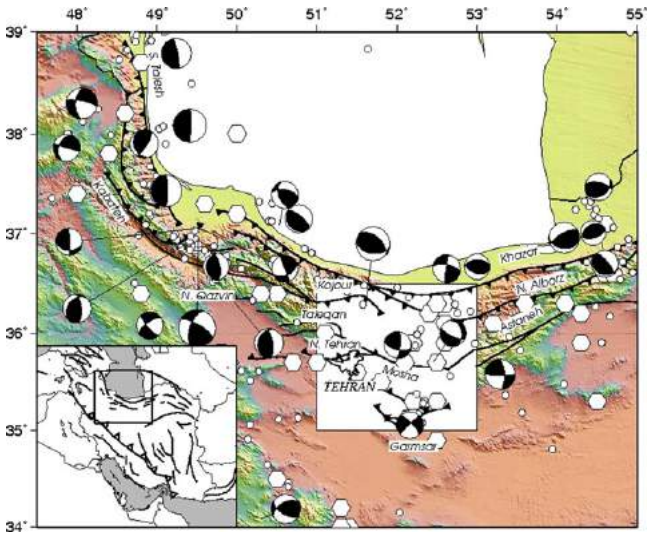

Fig. 1. Tectonic map of the Central Alborz. Faults are from Berberian and Yeats (2001) and Allen et al. (2003). Seismicity (Engdahl et al., 2006) is shown by open circles. Historical seismicity (Ambraseys and Melville, 1982) is presented as open hexagons. CMT focal mechanisms (http://www.seismology.harvard.edu/CMTsearch.html) are reported as black focal spheres. The white rectangle shows the location of the study region.

earthquakes recorded by permanent stations of different regional seismological networks during the same period.

We used a 1D inversion of first arrival times of local earthquakes and a joint inversion of receiver functions and fundamental mode of Rayleigh wave group velocity dispersion data to determine the crustal structure of the southern edge of the Central Alborz. Receiver functions are mostly sensitive to sharp velocity contrasts, and relatively insensitive to the average velocity or to smooth velocity gradients. Rayleigh wave group velocity is sensitive to the average shear velocity. Combining these complimentary tools in a single inversion allows a more detailed analysis of crustal and upper mantle structure and increases the uniqueness of the solution over separate inversions. It also facilitates explicit parameterization of layer thickness in the model space.

2. Geophysical and tectonics background

The Alborz range results from the collision of a piece of Gondwana with Eurasia in the late Triassic (Sengor et al., 1988). It forms a high arc of E–W trending mountains 60–120 km wide and ~600 km long in northern Iran. The mean elevation changes from 3000 m in the inner belt to −28 m at the Caspian shoreline. It is bounded by the Talesh Mountains to the west and by the Kopet Dagh Mountains to the east, and contains many summits in the range 3600–4800 m, including the Quaternary volcano of Damavand (5671 m) in the center of the belt (Fig. 1).

The Alborz accommodates the overall motion between the southern Caspian and Central Iran (Jackson et al., 2002). Its total shortening since the early Pliocene is estimated to be 30 km at the longitude of Tehran (Allen et al., 2003). The deformation of the Alborz is due to the northward shortening between the central Iranian Block and the Eurasian plate (Vernant et al., 2004).

The Central Alborz contains several active faults (Figs. 1 and 2), which strike parallel or sub-parallel to the range and accommodate the present-day oblique left-lateral shortening across the mountain belt (Berberian, 1983; Trifonov et al., 1996; Allen et al., 2003). In the northern Alborz, the most important faults (the Khazar and the North Alborz reverse faults) dip southward, whilst in the southern Alborz, the main active faults (the Mosha and the North Tehran faults) dip northward. One of the most important faults, the Mosha fault, which is located within our seismological network, is a left-lateral strike–slip fault about 180 km long. The Mosha fault and the Damavand stratovolcano are the two predominant features of the southern edge of the Central Alborz.

A number of authors have discussed destructive, historical earthquakes in the southern part of the Central Alborz, and in particular the Tehran region (e.g. Ambraseys and Melville, 1982; Berberian and Yeats, 2001). The largest events are associated with well-known faults either in the immediate vicinity of Tehran or in the Central Alborz to the North (Fig. 1). The Mosha fault seems to be one of the most active, experiencing earthquakes of magnitude greater than 6.5 in 958, 1665 and 1830 (Berberian and Yeats, 2001). Two large earthquakes (Ms > 7.0) are thought to have occurred on the Garmsar fault during the third century BC and in 743 (Ambraseys and Melville, 1982).

During the 20th century, no strong events were located in the southern part of the Central Alborz, but several events of magnitudes greater than 5 were associated with the Mosha fault in the immediate vicinity northeast of Tehran.

Most of the focal mechanisms computed from body wave modeling (Priestley et al., 1994; Jackson et al., 2002) or from the Global CMT catalogue show either reverse faulting or left-lateral strike–slip on faults parallel to the regional strike of the belt (Fig. 1). Most of the focal mechanisms computed from first arrival of local earthquakes (Ashtari et al., 2005) indicate left-lateral motion on the Mosha and Garmsar faults.

3. Data

The data used for the determination of the shallow velocity structure are P-wave arrival times of local earthquakes, mostly recorded by our temporary local seismological network of 44 short period stations. This network consisted of twenty-two stations equipped with TAD 12 bit digitizer, recording in a trigger mode at a sampling rate of 125 Hz and connected to a 2-Hz vertical seismometer, and thirteen CMG-6TD Guralp instruments with a 24-bit CMG-DM24 digitizer connected to a 3-component seismometer with frequency range between 10 s and 50 Hz. These stations operated in continuous mode at a sampling rate of 100 Hz. Our local

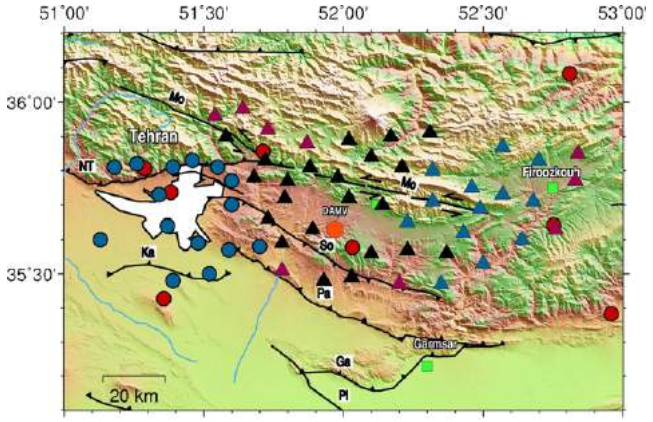

Fig. 2. Tectonic map of the Tehran region. Faults are from Allen et al. (2003). Some faults were mapped using SRTM digital topography data and satellite imagery in addition to field observations. Thrust faults (with teeth on the hanging wall) are marked as follows: NT for North Tehran fault, Ga for Garmsar fault, Pa for Parchin fault, Pi for Pishva fault, So for Sorkhe fault, and Ka for Kahrizak fault. The left-lateral Mosha fault (Mo) is marked by a line with no teeth. The temporary local seismological stations are triangles with different colors: TAD stations in black, MiniTitan stations in red, and CMG-6TD Guralp stations in blue. Red circles are the TDSN stations and blue circles are TDMMC stations operating as permanent networks in the region. The broad-band station, DAMV, is presented as orange circle in the middle of figure. (For interpretation of the references to colour in this figure legend, the reader is referred to the web version of the article.)

Table 1
Initial velocity model used for earthquakes location (Ashtari et al., 2005).

Depth range (km)	P-velocity (km/s)
0.0	5.4
2.0	5.7
8.0	6.0
12.0	6.3
35.0	8.0

network was completed by 9 MiniTitan recorders connected to a 5-s 3-component seismometer. The MiniTitan stations also record in a continuous mode at a sampling rate of 125 Hz (Fig. 2). The time was calibrated every hour by a GPS receiver connected to each station.

We also used data collected by permanent regional and local seismological networks in our study area. These networks include the Tehran Digital Seismological Network (TDSN) and the Mazandaran Digital Seismological Network (MDSN), which comprise twelve and five telemetry, short-period stations respectively, and are operated by the Institute of Geophysics, University of Tehran (IGUT). In addition, we used data from the permanent seismological network of the Tehran Disaster Municipality Management Center (TDMMC), which includes fifteen portable short-period stations (Fig. 2). We also used recorded local and teleseismic events at DAMV, one of the 3-component stations of the Iranian Broad-band Seismological Network (INSN).

All of the readings were picked using the Pickev (http://sismalp.obs.ujfgrenoble, Frechet and Thouvenot, 2000) and SEISAN (Havskov and Ottemöller, 2005) software. We estimate the picking accuracy to be better than 0.05 s for all readings.

For the determination of the Moho depth, we used more than one year of teleseismic waveforms located at epicentral distances of 30–90° and recorded at the DAMV broad-band station (INSN). Information about the group velocity dispersion comes from tomographic images between 10 s and 70 s period produced by a study of regional fundamental modes of Rayleigh waves propagating across Iran and surrounding regions (Rham, 2009).

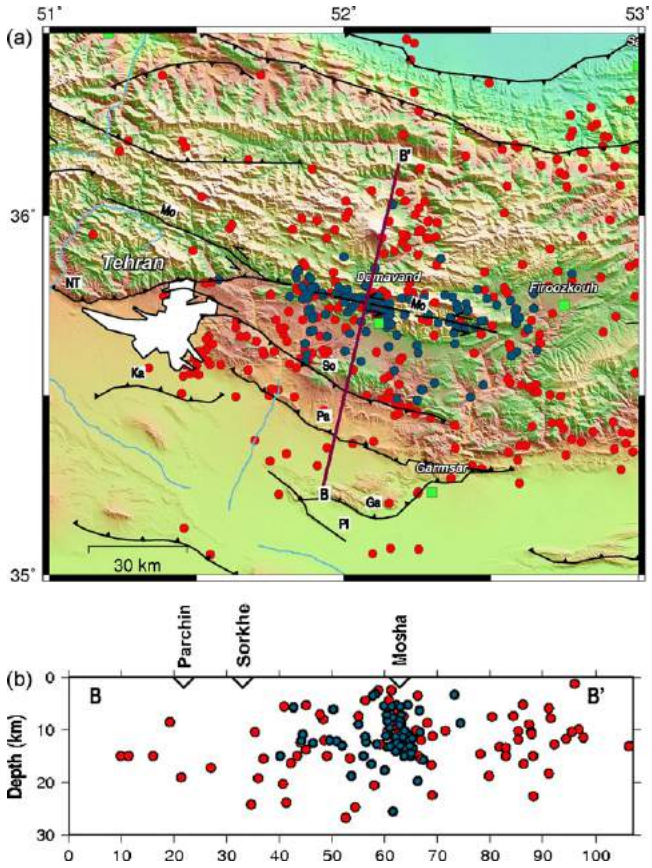

Fig. 3. (a) Local seismicity of 482 (red circles) and 115 (blue circles) selected earthquakes recorded by temporary and permanent seismological stations from June to December 2006. (b) Distribution of focal depths are presented on section BB' perpendicular to the seismicity; the surface traces of the Parchin, Sorkhe and Mosha faults are also shown. Seismicity is concentrated between depths of 2 km and 26 km. (For interpretation of the references to colour in this figure legend, the reader is referred to the web version of the article.)

4. Methodology

4.1. The shallow crustal structural

We first located all local events with Hypo71 (Lee and Lahr, 1972) and HYPOCENTER (Lienert, 1994). A total of 1144 seismic events were located using the velocity model of Ashtari et al. (2005) proposed for the study region (Table 1). We eliminated all the teleseismic and regional events and most of the explosions from our total dataset, which comprised 1144 seismic events. From the remaining events, we selected a subset of 482 local earthquakes with hypocentral errors less than 5 km (Fig. 3). Among these events, we selected 115 well located earthquakes recorded by a minimum of 8 stations, having horizontal and vertical errors in location less than 3 km, with an azimuthally gap less than 180° and a RMS value less than 0.3 s. These 115 events were used to conduct several tests for the determination of the velocity structure. Distributions of both selected subsets indicate that most of the seismicity is located on the Mosha fault at depths of between 3 km and 20 km (Fig. 3). Using 2780 P and S phases from the 115 selected events, we computed a mean V_p/V_s ratio of 1.734 ± 0.005 by averaging the $T_{Si} - T_{Sj}$ vs. $T_{Pi} - T_{Pj}$.

Secondly, we inverted the arrival times of the selected set of events for a 1D velocity structure using the program VELEST (Kissling, 1988). Because the resulting structure is strongly dependent on the starting velocity model, we explored 100 initial models randomly distributed around our starting model (with differences as large as 0.5 km s^{-1} in each layer). We kept only the resulting models for which the RMS decreased significantly. The inversion procedure was done in two steps: first we used a starting velocity structure composed of a stack of layers 2 km thick, of uniform velocity 6.0 km s^{-1}. The result of these inversions (Fig. 4a) suggests that no more than five layers are required in the starting model. In a second step, the five-layer model was randomly perturbated, to obtain a set of initial models for the inversions. The final velocity model was computed averaging the results of all inversions that converge properly (Fig. 4b and Table 2). We also checked, with the selected set of data, that the corresponding RMS value reduced from 0.32 s for the starting homogeneous model, to 0.21 s for the final five-layer model.

The shallowest ~3 km thick layer with a P-wave velocity of 5.4 ± 0.05 km s^{-1} is present in all our final 1D velocity models. It likely represents the shallow sedimentary layers. From ~3 km to ~7 km depth, the velocity is greater at 5.8 km s^{-1}, probably

Table 2
1D velocity structure.

	P-velocity (km/s)
0.0	5.40
3.0	5.80
7.0	6.10
16.0	6.25
24.0	6.40

Maximum error in depth range = ±1 km. Maximum error in P-velocity = ±0.05 km/s.

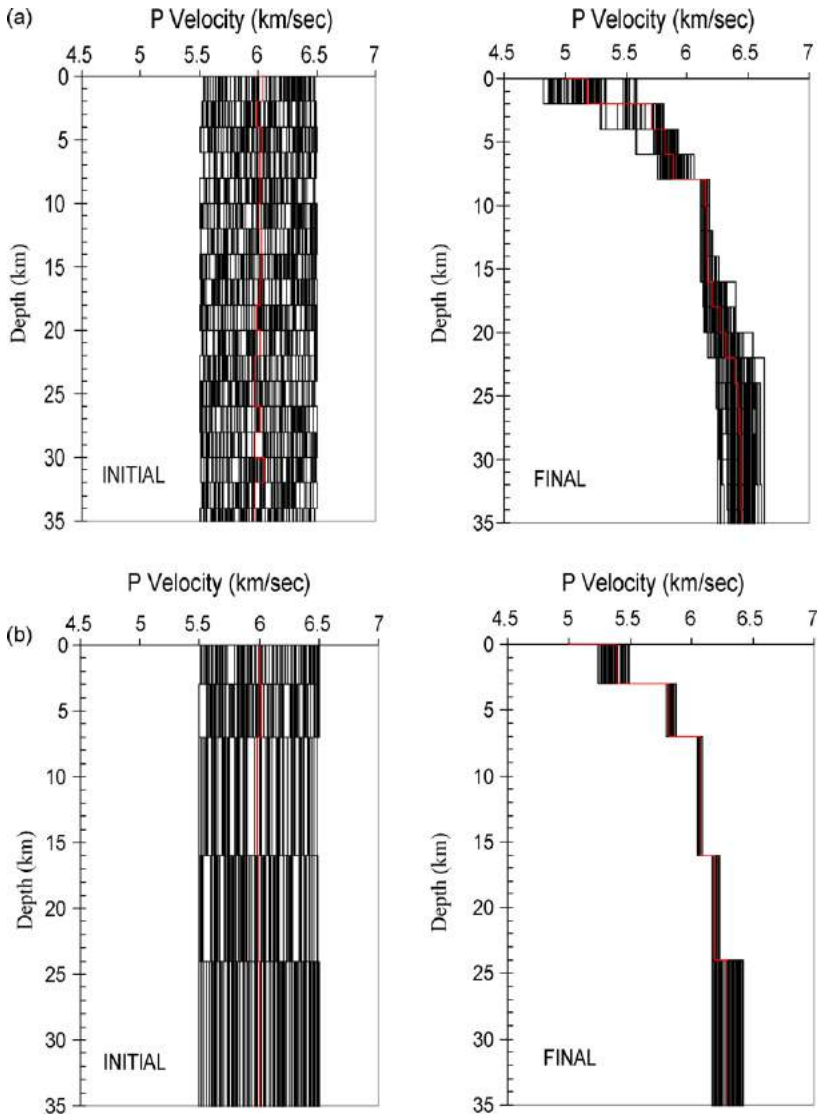

Fig. 4. Velocity structure obtained for the shallow crust by 1D inversion of travel times (Kissling, 1988) of the 115 selected aftershocks recorded by a minimum of 8 seismological stations. We use 100 randomly distributed starting models (left) that converge to the models plotted in the right hand side. (a) Model with 17 layers, 2 km thick. (b) Simplified five-layer starting model.

reflecting an increase in the density of older sediments. Below the sedimentary cover, our model consists of two layers ~9 km and ~8 km thick with P-wave velocities of ~6.10 and 6.25 km s^{-1}, respectively. The combined thickness of these layers (17 km) probably represents the upper crystalline crust. Our model shows a fairly well-constrained interface at ~24 km depth, below which V_p increases to ~6.40 km s^{-1}. This is probably the interface between the lower and the upper crystalline crust, although the velocity of the lower crust is not well determined because only a few events were located within or below this layer and very few propagation paths sampled the lower crustal layer. We also estimated the shallow velocity structure by exploring a wide range of reasonable velocity models for the crust, and minimizing the mean rms residual for a constant set of earthquakes and arrival times. The results are similar to what have been presented in Table 2.

4.2. The deep crustal structure

We jointly inverted teleseismic radial component receiver functions and regional Rayleigh wave group velocities for velocity structure beneath station DAMV, one of the broadband stations of Iranian National Seismic Network (INSN) which is located in the southern part of the Alborz tectonic zone.

The teleseismic receiver function is an efficient seismic tool for imaging horizontal interfaces (Langston, 1979). Modeling the amplitude and timing of receiver functions can supply valuable constraints on the depth of the interface. The time-domain iterative deconvolution procedure of Ligorria and Ammon (1999), which has higher stability with noisy data compared to frequency-domain methods, was employed to deconvolve the vertical component of the teleseismic P waveforms from the corresponding horizontal components and obtain radial and transverse receiver functions at DAMV broadband station. More than 120 teleseismic waveforms, recorded at this station from June 2004 to August 2005, were selected in order to obtain receiver function estimates for the station. We corrected the waveform from the instrument response before proceeding with the receiver function deconvolution. High-frequencies were filtered using a Gaussian filter, at 2.5 and 1.0, which gives an effective high-frequency limit of about 1.2 and 0.5 Hz respectively. As the structure may vary with azimuth and with epicentral distance, we grouped the observations by azimuth (<10°) and distance (Δ < 10°). To increase the signal-to-noise ratio

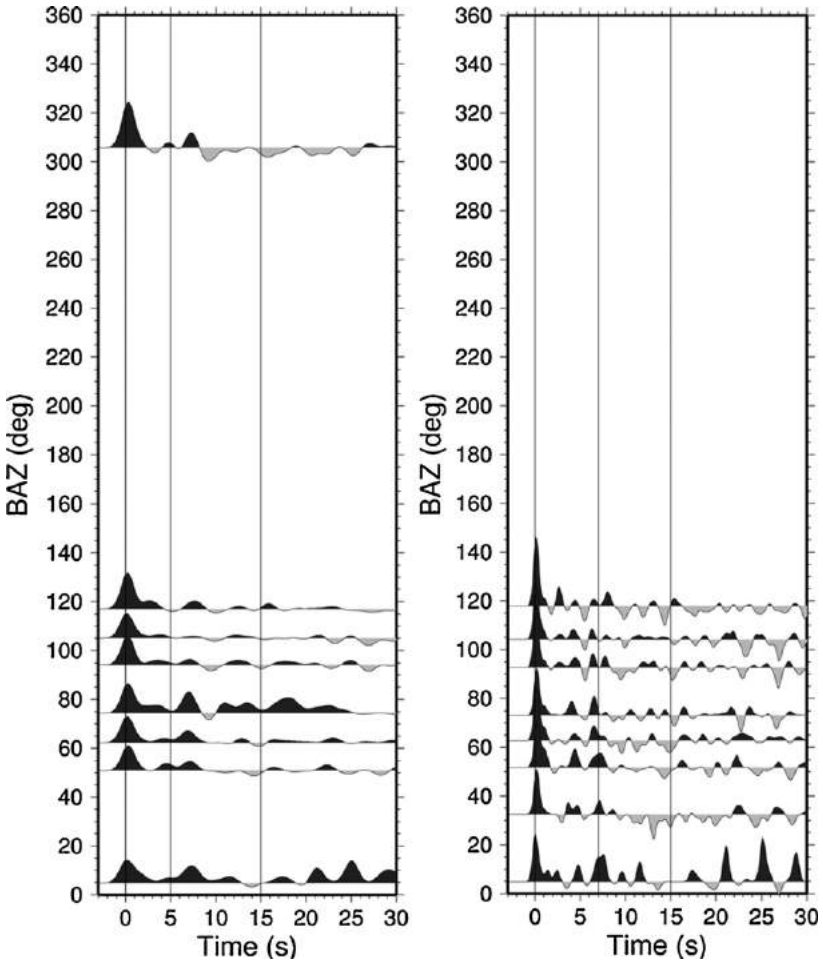

Fig. 5. Stacked radial receiver functions for DAMV station listed for each of the two Gaussian filter parameter 1.0 (left) and 2.5 (right). All events are generated using iterative deconvolution.

of the deconvolved traces, the individual receiver functions were aligned according to the P-wave arrival and point-to-point stacked waveforms. The stacked receiver function was then allocated the average slowness and back-azimuth of every event included in the stack. Fig. 5 shows the resultant radial receiver functions for each of the two Gaussian filter parameters.

Surface waves velocity dispersion primarily depends on S-velocity, with some dependence on P-velocity, and little dependence on density (Ozalaybey et al., 1997). They have been shown to improve inversions of receiver functions for crustal structure (Julia et al., 2000). Surface waves velocity dispersion provide information on the absolute seismic shear velocity, but are relatively insensitive to sharp velocity changes. The group velocities were incorporated into our joint-inversion scheme from an independent surface wave tomography study by Rham (2009). Group velocities from regional events recorded at permanent and broad-band stations were measured for fundamental-mode Rayleigh waves within the 10–70 s period range. The region was parameterized using a uniform, $1^\circ \times 1^\circ$, grid of constant-slowness cells. The dispersion curve is the result of tomographic imaging for each period separately. Fundamental-mode Rayleigh wave group velocities to station DAMV are taken from the corresponding tomographic cell containing the station.

Both the Rayleigh wave and receiver function energy are found in the P-SV plane and are therefore sensitive to V_{SV} in the crust, whereas the Love wave is restricted to the SH plane. This means both datasets are sampling the same crustal parameter. However, receiver functions constrain velocity contrasts and relative vertical travel times beneath the recording station, while dispersion velocities constrain average absolute S-wave velocity values within frequency-dependent depth ranges. The relative character of the receiver function constraints makes the inversion problem implicitly non-unique (Ammon et al., 1990), but this limitation can be overcome by incorporating the constraints on the absolute velocities from the dispersion estimates (Julia et al., 2000). The data sets are thus complementary.

The simultaneous inversion of two datasets to find a single velocity model was carried out using the Computer Program in Seismology software package (Herrmann and Ammon, 2003). This finds a single velocity structure by minimizing the following objective function:

$$S = \frac{1-p}{N_r}\sum_{i=0}^{N_r}\left(\frac{O_{ri}-P_{ri}}{\sigma_{ri}}\right)^2 + \frac{p}{N_s}\sum_{j=0}^{N_s}\left(\frac{O_{sj}-P_{sj}}{\sigma_{sj}}\right)^2$$

where S is observed receiver function at time t_i, O_{ri} is observed receiver function at time t_i, P_{ri} is standard error of observation at t_i, σ_{ri} is standard error of observation at t_i, O_{sj} is jth observed surface wave dispersion, P_{sj} is jth predicted surface wave dispersion point, σ_{sj} is standard error of jth surface wave observation, N_r is total number of receiver function points, N_s is total number of surface wave dispersion points, p is influence factor, $0 \le P \le 1$, $p = 0$: forces receiver function solution, $p = 1$: forces surface wave solution.

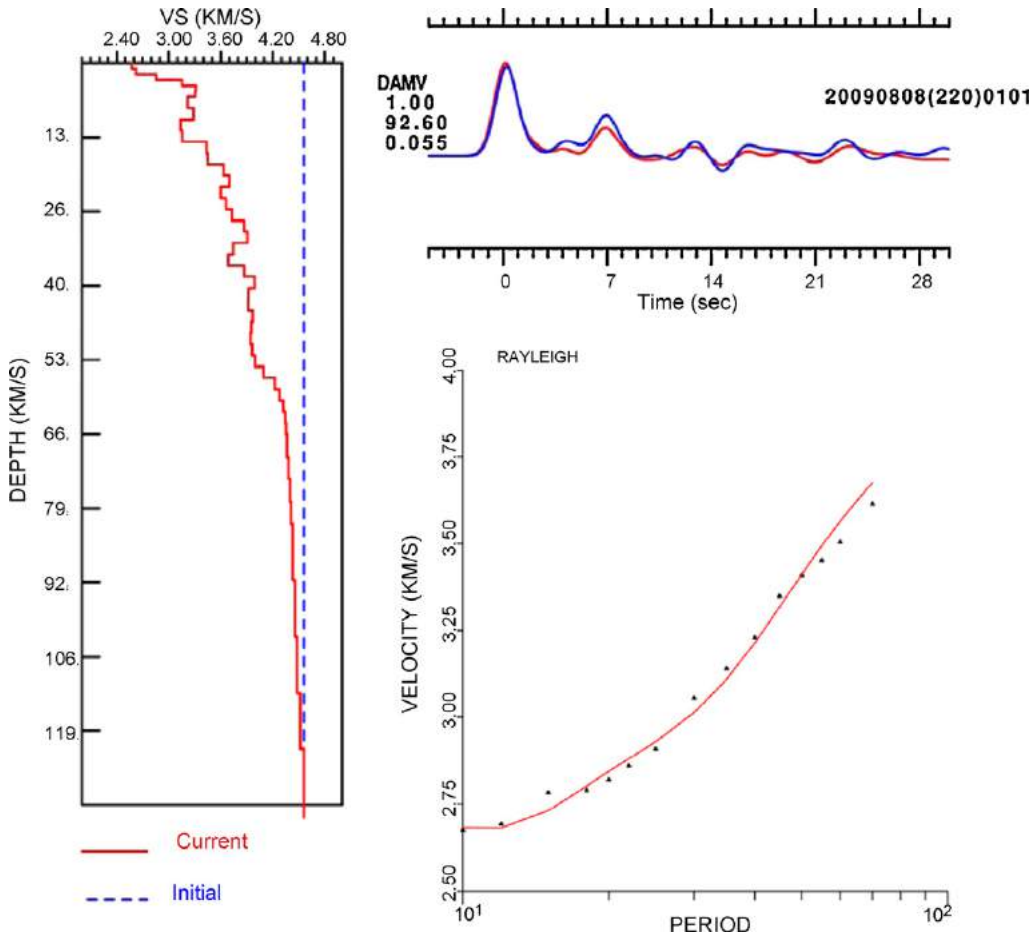

Fig. 6. Joint inversion results for station DAMV for 62° back-azimuth receiver function stack. The receiver function is at the top-right, the surface wave dispersion at the bottom-right, and the model at the left. The blue dashed line denotes the data and the red solid line the predictions for the model at the left. (For interpretation of the references to colour in this figure legend, the reader is referred to the web version of the article.)

The weighting refers to the statistical significance given to the receiver function data (S_{rf}) and surface data (S_{sw}), such that $S_{rf} + S_{sw} = 1$.

The inversion package requires that the real velocity structure be represented by a set of flat-lying, homogeneous, isotropic velocity layers, and that during inversion the vertical extent of each layer remains fixed, whereas the velocity is free to change (within user-defined damping limits). The starting model comprised layers that were 1 km thick for the top 6 km of the model space, 2 km thick between 6 and 66 km, and 4 km thick between 66 and 78 km. The starting velocity for each layer in the model was $V_p = 8.0$ km/s, which equates to upper mantle velocities.

Among more than 120 computed receiver functions using a Gaussian parameter of 1, 8 receiver function stacks were made for 41 good quality, acceptable receiver functions with clear Ps converted phases (Fig. 5). We modeled the crustal velocity structure for all the stacked receiver functions with different back azimuths, and a total of 5 models were acceptable finally. We ran joint inversions with $p = 0.1$–0.9 range to find the best match of observed and predicted receiver function/surface wave. Our preferred results were for $p = 0.2$, as it provided the best fit for both receiver function and dispersion curve. Fig. 6 shows the joint inversion results for a receiver function stack with a mean back-azimuth of 62°. This stack contains 5 events with epicentral distances of 67–76° and back azimuth range between 59° and 68°. The radial receiver function and the surface wave dispersion curve are shown at the upper and lower right panels, respectively. The left panel shows the initial and estimated velocity model. The blue dashed line denotes the data and the red solid line the predictions for the model at the left. From this figure, we infer that the Ps delay time is nearly 7 s. The fit to both observed and predicted receiver functions and observed and predicted group velocities dispersion values are good.

4.3. Simplification of the model

The final crustal velocity model of Fig. 6 gives a complex crustal structure beneath the Southern flank of Alborz. It is important to establish how much of the complexity seen in the model results from the fitting of noise in the receiver function and surface wave data. In order to eliminate unnecessary complexity, we simplified the model resulted from the previous step by amalgamating the 2 km thick layer with the same velocity as thicker layer. However, we took care that the simplest resulting model fitted the observed data. The process, shown in Fig. 7, takes the output model of the joint inversion (Fig. 6) and fits the simplest five layered model to it. Synthetic dispersion curves and receiver functions are produced for this layered half space, and compared to both the original data, and those produced by the joint inversion. As an error analysis, the resolution of the final simple crustal model was tested by offsetting the Moho by ±10 km, ±5 km, ±2 km, and ±1 km from the model-determined Moho depth. Synthetics were then produced for this new model and compared to the final model results, the joint inversion and the original data. This approach showed that the Moho could be offset up to ±2 km, before the synthetics had varied away from the data by such a degree as to be visually different. In this way, we estimated errors of 2.0 km

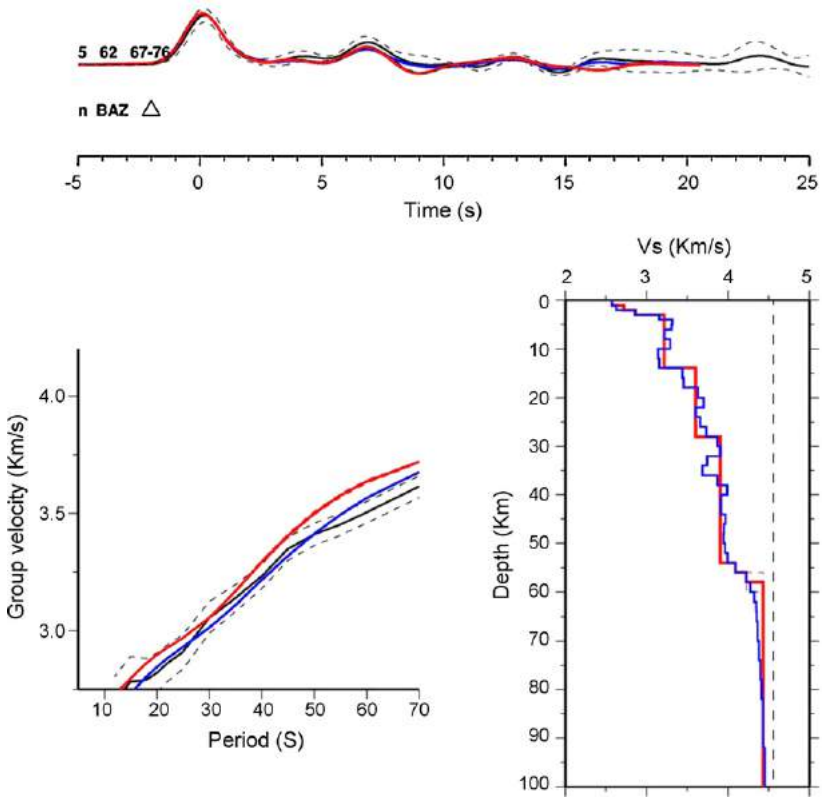

Fig. 7. Forward modeling results for the receiver structure at DAMV based on the receiver function stack with a mean back-azimuth of 62°. This stack contains 5 events which range in epicentral distances 67–76°. The original receiver function and dispersion curve (solid black lines) and their associated standard deviations (black dashed) are shown, along with the receiver function and dispersion curve for the joint inversion model (blue) and the simplified forward model, synthetic receiver function and synthetic dispersion curve for the forward modeling (red). The initial model used for the joint inversion is shown in black dashed line. The receiver function is at the top, the surface wave dispersion at the bottom-left, and the model at the right. (For interpretation of the references to colour in this figure legend, the reader is referred to the web version of the article.)

on the calculated Moho depth for each stacked receiver function.

The results for five acceptable receiver function stacks are summarized in Fig. 8. For each stacked receiver function, we used the output model of the joint inversion as a starting model, and tried to fit the simplest four or five layered model to it.

As can be observed in Fig. 8, all the models contain a thin (~3–5 km) layer of low-velocity material (V_s < 3.2 km/s) below the surface, overlaying a rapid velocity increase of 3.2 km/s. In most of the models, we observe two interfaces with sharp velocity increases at ~16 km and ~26 km, a lower crust with a rather constant velocity, and a gradational crust-to-mantle transition. The Moho discontinuity is composed of a series of small velocity steps located at 58 ± 2 km depth. In most of the models, the crust-to-mantle transition zone is imaged as a velocity increase of ~0.3–0.4 km/s over a 4 km depth interval.

We also computed the receiver function using a Gaussian parameter (α) of 2.5. This filter is supposed to remove high frequency noise by low-pass filtering the results at 1.2 Hz. So, the computed receiver functions contain quite high frequencies compared to previously described receiver functions filtered at 0.5 Hz (α = 1.0).

We followed the same procedure described earlier for selecting and stacking the acceptable receive functions. As expected, the stacked receiver functions contain high frequencies (Fig. 5), which impose more complexity in the resulted crustal structure. However, we tried jointly inverting them with Rayleigh wave, group velocity dispersion data. First, we used the 2 km thick, multilayered model with a constant velocity of V_s = 4.6 km/s as an initial model. The resulting model was very complex, indicating many velocity interfaces. In a second step, we minimized the unknown parameters by simplifying the multilayered model from the joint inversion in four or five layered models, as described earlier. We tried to show that the goodness of fit is still high for new computed receiver functions (α = 2.5). For most of the different back azimuth stacks, both the initial multilayer (from joint inversion) and the simplified model provide a reasonable fit to the observed receiver function and dispersion curve (Fig. 9). Although the Ps conversions at the Moho depth are different, Fig. 9 indicates very similar results as were obtained for the previous data set (α = 1.0). In most of the models, the crust-to-mantle transition zone is composed of a series of small velocity steps located at 55 ± 2 km depth.

5. Discussion

We computed the crustal model for a region located on the southern flank of the Central Alborz near Tehran. Our model may not be valid for the entire Central Alborz, due to the existence of important lateral variations in the structure that we expect for such a complex orogenic belt. However, it is the most reliable crustal structure based on the seismological constraints east of Tehran.

The shallow crust beneath the study region consists of a 7 km thick sedimentary layer overlying a 17 ± 2 km thick upper crystalline layer. The sedimentary cover consist of a thin layer 3 km thick (V_p ~ 5.4 km s^{-1}) over a 4 km thick layer (V_p ~ 5.8 km s^{-1}). The crystalline crust consists of three layers: an upper layer extending from ~7 to ~16 km depth (V_p ~ 6.1 km s^{-1}), a middle layer extending from ~16 to ~24 km (V_p ~ 6.25 km s^{-1}), and a lower layer extending from ~24 to the Moho (V_p ~ 6.40 km s^{-1}). The first two crystalline layers are associated with the upper crystalline crust.

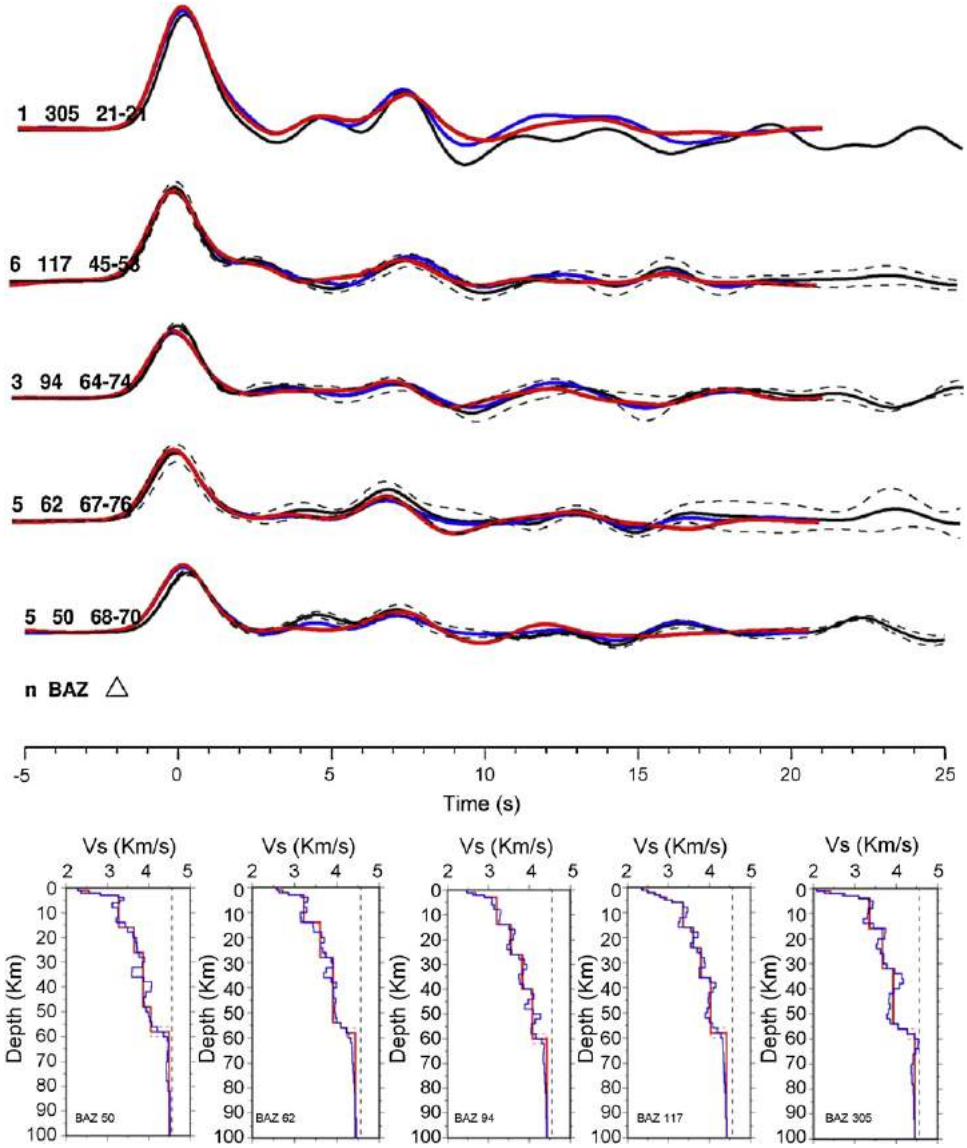

Fig. 8. Forward modeling results for the receiver structure at DAMV based on five acceptable receiver function stacks. For each stacked receiver function, we used the output model of the joint inversion as a starting model, and tried to fit the simplest four or five layered model to it. Format of the plot is the same as for Fig. 7.

The upper and lower crystalline crust interface is located at a depth of ~24 km (Table 2). The accuracy of the velocity estimates is likely $\pm 0.1\,km\,s^{-1}$, which ensures robust identification of the different interfaces between the sediments and the metamorphic crust.

Only sparse, reliable information is available regarding the shallow crust of the Southern Alborz. Using microearthquakes recorded by a temporary local seismological network operating for seven weeks around Tehran, in addition to data from the permanent Tehran Digital Seismic Network (TDSN), Ashtari et al. (2005) investigated the velocity model for the region around Tehran. They used arrival times of 36 earthquakes that were recorded during their two temporary experiments and estimated that the crust consists of a very thin, 2-km thick layer ($V_p \sim 5.4\,km\,s^{-1}$) over a 6 km thick layer ($V_p \sim 5.7\,km\,s^{-1}$), both assumed to be sedimentary. Based on their results the crystalline crust consists of two layers 4 and 23 km thick with P-wave velocities of 6.0 and $6.3\,km\,s^{-1}$ respectively (Table 1). They estimated a depth of 35 km for the Moho discontinuity beneath the study area.

Our results are very similar to those obtained by Ashtari et al. (2005) except for the two last interfaces. Our results support somewhat deeper interfaces at ~16 and ~24 km depth, while they reported only one interface at 12 km. Relocation of 482 selected earthquakes using our model resulted in an average rms of time residual about 0.16 s, while it gave the values of 0.19 s when we relocated them with the velocity model of Ashtari et al. (2005). The average of horizontal (erh) and vertical (erz) errors decreased 1.1 and 6.4 km respectively when we relocated 482 events using our velocity model instead of initial Ashtari et al. (2005) model. We consider our results to be more reliable as our data set used for 1D inversion of first arrival times includes better-constrained events which ensure better constraints on the interfaces and velocities in our crustal velocity structure.

We have determined the deep crustal velocity structure beneath the south margin of the Central Alborz by simultaneously inverting receiver function data and fundamental mode Rayleigh wave group velocity measurements. These analyses show a thickness of 58 ± 2.0 km for the crust beneath the study region. Although the receiver function technique is efficient for the detection of strong contrasts such as the Moho, we observed a good consistency between the results of one-dimensional inversion and the joint inversion of receiver function and surface wave dispersion for the detection of crustal interfaces. The joint inversion tech-

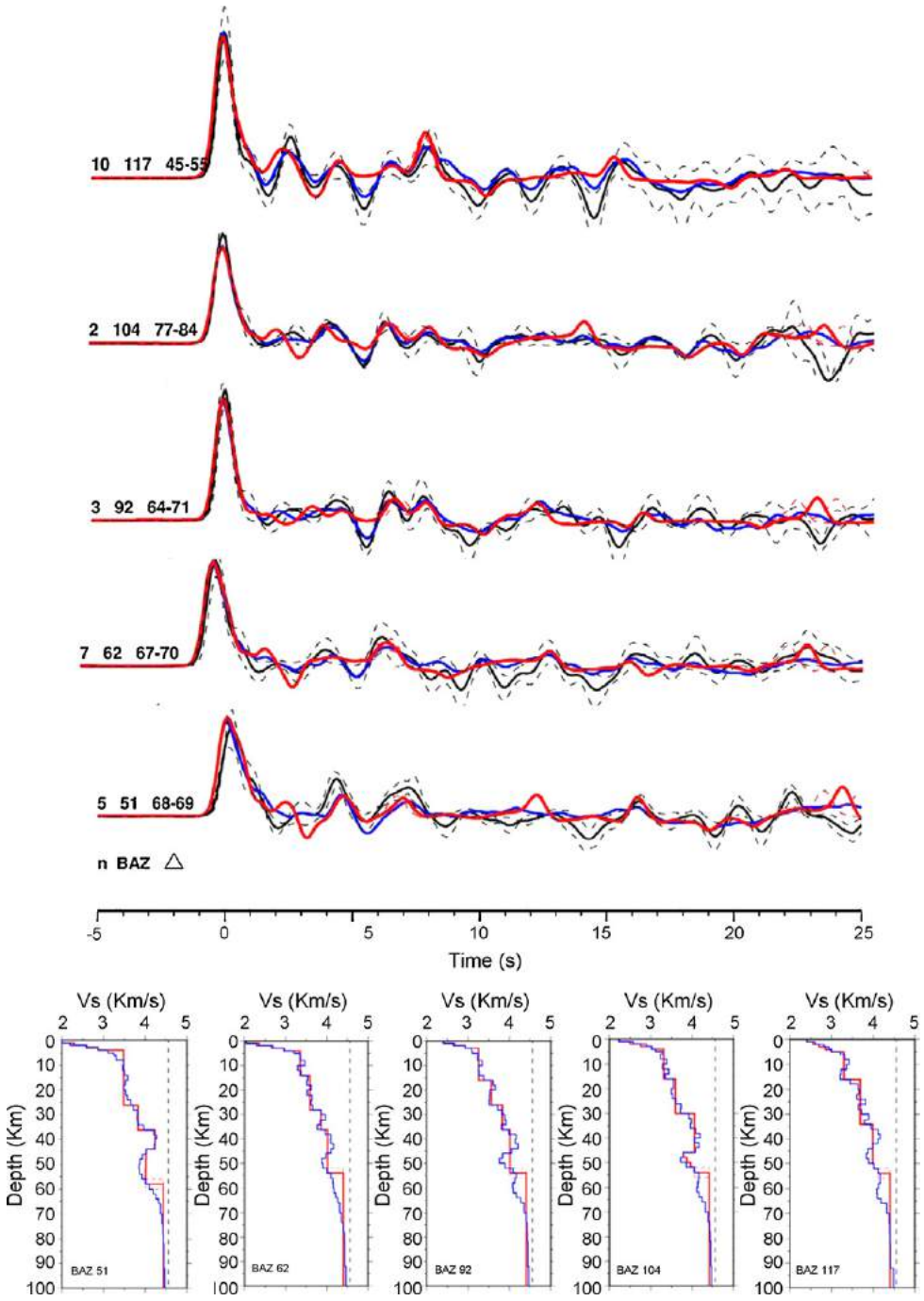

Fig. 9. Forward modeling results for the five receiver function stacks computed with Gaussian parameter of 2.5. As we observe for most of the different back azimuth stacks, both the initial multilayer (from joint inversion) and the simplified model provide a reasonable fit to the observed receiver function and dispersion curve. Format of the plot is the same as for Fig. 7.

nique applied on teleseismic events therefore provided useful and complementary information for better constraining shallower discontinuities in addition to determining the Moho depth. In particular, the identification of an interface at ~26 km depth, which was not constrained well by local earthquakes, helped us to distinguish the upper and lower crystalline crust interface. Another crustal interface clearly observed in most of the modeled stacked receiver functions is at ~16 km depth, and is consistent with the shallow crustal structure determined from 1D inversion of local earthquakes travel times.

Recently, Sodoudi et al. (2009) studied the crust and mantle lithosphere beneath the Central Alborz region using P- and S-receiver function methods. They estimated a thick crust of ~67.5 km in the region beneath the DMV short period station (which is located close to the DAMV broadband station used in this study). They observed two coherent conversion phases at 6.2 and 7.8 s, and they concluded the second one is the Ps conversion at the Moho depth. In this regard we agree with them as our receiver functions show a clear Ps conversion at ~7 s and ~7.8 for Gaussian parameters of 1.0 and 2.5, respectively. However, we believe that the difference of ~9 km in the estimated crustal thickness is mainly due to the difference in velocity profile they used for converting their Ps delay times to an interface conversion depth. They used the IASPEI91 reference model (Kennett and Engdahl,

Table 3
IASPEI 91 velocity model (Kennett and Engdahl, 1991).

Depth range (km)	P-velocity (km/s)
0.0	5.8
20.0	6.5
35.0	8.0

1991), whose velocities are higher than local velocities we obtained for the southern edge of the Central Alborz. The IASPEI91 model is presented in Table 3. In spite of a good consistency between the results of 1D inversion of local earthquake travel times and joint inversion of teleseismic receiver function and surface wave dispersion data, IASPEI91 shows considerably higher velocities, especially for the lower crystalline crust. Using this faster model (average V_S 3.90 km s^{-1}) comparing to our velocity model (average V_S 3.58 km s^{-1}) will result in 5–6 km deeper Moho estimation from Ps conversion. In this study, we minimized the effect of non-uniqueness of the receiver function analysis and the problem of under- or over-estimating the velocity information by simultaneously inverting the receiver functions with Rayleigh wave group velocity dispersion data.

Our results from joint inversion of receiver functions and Rayleigh wave dispersion curves indicate that the velocity of the upper crystalline crust beneath the southern margin of the Central Alborz is more than beneath the central Zagros (Hatzfeld et al., 2003). We obtained an average thickness of 51 km for the crystalline crust and a Moho depth of 58 ± 2 km beneath the southern foothills of the Central Alborz, which is more than the 35 km thickness of the crystalline crust and the 46 km depth of the Moho beneath the central Zagros.

6. Conclusion

Using arrival times of local earthquakes recorded by a dense seismological network, we infer the upper-crust velocity structure to be composed of a 7 km thick sedimentary layer and a 17 km thick upper crystalline crust. Joint inversion of receiver functions and Rayleigh wave dispersion data of 42 teleseismic earthquakes suggests a 34 ± 2 km thick lower crust of 6.4 km s^{-1} velocity. These estimates, obtained with reasonable amounts of data, are the most reliable, quantitative, seismological estimates for the southern flank of the Central Alborz. The total thickness (~51 km) of the crystalline crust therefore looks much more than the ~35 km thickness of the central Zagros and the stretched margin of the Arabian Platform (Hatzfeld et al., 2003), indicating that there has been more extensive shortening and crustal deformation in this region than in the Zagros. We believe that the results of this study can improve the routine earthquake location of the TDSN and TDMMC networks. As the seismic hazard assessment strongly depends on the accuracy of earthquake locations, our results should greatly influence seismic hazard evaluation in the southern part of the Central Alborz.

Acknowledgements

We thank the observers and drivers who helped us in the field. MT acknowledges visiting support from the Earth Sciences Department, University of Cambridge. We thank Daniel Rham for providing the Rayleigh wave group velocity dispersion data. We would like to thank Ed Nissen for grammatical edits and corrections. This research is supported by the International Institute of Earthquake Engineering and Seismology (IIEES) and partially by the French ANR Catell. The stations belong to the French national pool of mobile seismic instruments Sismob with complement from IIEES. We thank the former president of IIEES, Prof. Ghafory-Ashtiany for his constant support. We thank two anonymous reviewers for helpful reviews. We used the Computer programs in seismology (Herrmann and Ammon, 2003) for data processing and GMT (Wessel and Smith, 1995) for plotting.

References

Allen, M.B., Ghassemi, M.R., Sharabi, M., Qoraishi, M., 2003. Accommodation of late Cenozoic oblique shortening in the Alborz range, northern Iran. Journal of Structural Geology 25, 659–672.
Ambraseys, N.N, Melville, C.P., 1982. A history of Persian earthquakes. In: Cambridge Earth Science Series. Cambridge University Press, London, 212 pp.
Ammon, C.J., Randall, G.E., Zandt, G., 1990. On the non-uniqueness of receiver function inversions. Journal of Geophysics Research 95, 15303–15318.
Ashtari, M., Hatzfeld, D., Kamalian, N., 2005. Microseismicity in the region of Tehran. Tectonophysics 395, 193–208.
Asudeh, I., 1982. Seismic structure of Iran from surface and body wave data. Geophysical Journal of Research Astronomical Society 71, 715–730.
Berberian, M., 1983. The southern Caspian: a compressional depression floored by a trapped, modified oceanic crust. Canadian Journal of Earth Sciences 20, 163–183.
Berberian, M., Yeats, R.S., 2001. Contribution of archaeological data to studies of earthquake history in the Iranian plateau. Journal of Structural Geology 23, 563–584.
Dehghani, G.A., Makris, J., 1984. The gravity field and crustal structure of Iran. Neues Jahrb. Geological Paleontology 168, 215–229.
Engdahl, E.R., Jackson, J.A., Myers, S.C., Bergman, E.A., Priestley, K., 2006. Relocation and assessment of seismicity in the Iran region. Geophysical Journal International 167, 761–778.
Frechet, J., Thouvenot, F., 2000. PICKEV 2000 Software, Copyright© 1993–2006, the Joseph Fourier University (UJF) and the National Center for Scientific Research (CNRS), SISMALP Network.
Hatzfeld, D., Tatar, M., Priestley, K., Ghafory Ashtiani, M., 2003. Seismological constraints on the crustal structure beneath the Zagros Mountain belt (Iran). Geophysical Journal International 155, 1–8.
Havskov, J., Ottemöller, L., 2005. SEISAN: the earthquake analysis software for windows, solaris, Linux and Macosx, Version 8.1.
Herrmann, R.B., Ammon, C.J., 2003. Computer programs in seismology, version 3.20, surface waves. In: Receiver Functions and Crustal Structure. Saint Louis University, Penn State University.
Jackson, J.A., Priestley, K., Allen, M.B., Berberian, M., 2002. Active tectonics of the South Caspian Basin. Geophysical Journal International 148, 214–245.
Javan Doloei, G., Roberts, R., 2003. Crust and uppermost mantle structure of Tehran region from analysis of teleseismic P-waveform receiver functions. Tectonophysics 364, 115–133.
Julia, J., Ammon, C.J., Herrmann, R.B., Correig, A.M., 2000. Joint inversion of receiver function and surface-wave dispersion observations. Geophysical Journal International 143, 99–112.
Kennett, B.L.N., Engdahl, E.R., 1991. Traveltimes for global earthquake location and phase identification. Geophysical Journal International 105, 429–465.
Kissling, E., 1988. Geotomography with local earthquake data. Review of Geophysics 26, 659–698.
Langston, C.A., 1979. Structure under Mount Rainier, Washington, the inferred from teleseismic body waves. Journal of Geophysics Research 84, 4749–4762.
Lee, W.H.K., Lahr, J.C., 1972. HYPO71 (Revised): a computer program for determining hypocenter, magnitude, and first motion pattern of local earthquakes. United States Geological Survey Open File Report 75-311, 113 pp.
Lienert, B.R., 1994. HYPOCENTER 3.2: A Computer Program for Locating Earthquakes, Locally, Regionally and Globally. Hawaii Institute of Geophysics & Planetology, 2525 Corea Rd, Honolulu, HI, 74 pp.
Ligorria, J.P., Ammon, C.J., 1999. Iterative deconvolution and receiver function estimation. Bulletin of the Seismological Society of America 89, 1395–1400.
Ozalaybey, S., Savage, M.K., Sheehan, A.F., Louie, J.N., Brune, J.N., 1997. Shear-wave velocity structure in the northern basin and range province from the combined analysis of receiver functions and surface waves. Bulletin of the Seismological Society of America 87, 183–199.
Paul, A., Kaviani, A., Hatzfeld, D., Tatar, M., 2009. Seismic imaging of the lithospheric structure of the Zagros mountain belt, submitted to "Tectonic and Stratigraphic evolution of Zagros and Makran during the Meso-Cenozoic", P. Leturmy & C. Robin (Eds.), Geol. Soc. London Spec. Pub.
Priestley, K., Baker, C., Jackson, J., 1994. Implications of earthquake focal mechanism data for the active tectonics of the south Caspian basin and surrounding regions. Geophysical Journal International 118, 111–141.
Radjaee, A.H., 2007. The crustal structure in the Central Alborz from receiver functions analysis. Ph.D. Thesis. International Institute of Earthquake Engineering and Seismology.
Radjaee, A.H., Rham, D., Mokhtari, M., Tatar, M., Priestley, K., Hatzfeld, D. Variation of Moho depth in the Central part of Alborz Mountains, North of Iran. Geophysical Journal International, submitted for publication.
Rham, D., 2009. The crustal structure of the Middle East. Ph.D. Thesis. University of Cambridge Library, Cambridge, UK.

Ritz, J.F., Nazari, H., Ghassemi, A., Salamati, R., Shafei, A., Solaymani, S., Vernant, P., 2006. Active transtension inside Central Alborz: a new insight into northern Iran–southern Caspian geodynamics. Geology 34, 477–480.

Sengor, A.M.C., Altiner, D., Cin, A., Ustaomer, T., Hsu, K.J., 1988. In: Audley-Charles, M.G., Hallam, A. (Eds.), Origin and Assembly of the Tehyside Orogenic Collage at the Expense of Gondwana Land. Geological Society of London, Sp., No. 37, pp. 119–181.

Sodoudi, F., Yuan, X., Kind, R., Heit, B., Sadidkhouy, A., 2009. Evidence for a missing crustal root and a thin lithosphere beneath the Central Alborz by receiver function studies. Geophysical Journal International 177, 733–742.

Trifonov, V.G., Hessami, K.T., Jamali, F., 1996. West-Trending Oblique Sinistral-Reverse Fault System in Northern Iran, vol. 75. IIEES Special Publication, Tehran, Iran.

Vernant, P., Nilforoushan, F., Chéry, J., Bayera, R., Djamour, Y., Masson, F., Nankali, H., Ritz, J.-F., Sedighi, M., Tavakoli, F., 2004. Deciphering oblique shortening of Central Alborz in Iran using geodetic data. Earth and Planetary Science Letters 223, 177–185.

Wessel, P., Smith, W.H.F., 1995. New version of the generic mapping tools released, EOS. Trans. Am. geophys. Un. 76, 329.